



HAL
open science

Tracing isomanifolds in R^d in time polynomial in d

Jean-Daniel Boissonnat, Siargey Kachanovich, Mathijs Wintraecken

► **To cite this version:**

Jean-Daniel Boissonnat, Siargey Kachanovich, Mathijs Wintraecken. Tracing isomanifolds in R^d in time polynomial in d . 2020. hal-03006663v1

HAL Id: hal-03006663

<https://inria.hal.science/hal-03006663v1>

Preprint submitted on 16 Nov 2020 (v1), last revised 17 Mar 2021 (v3)

HAL is a multi-disciplinary open access archive for the deposit and dissemination of scientific research documents, whether they are published or not. The documents may come from teaching and research institutions in France or abroad, or from public or private research centers.

L'archive ouverte pluridisciplinaire **HAL**, est destinée au dépôt et à la diffusion de documents scientifiques de niveau recherche, publiés ou non, émanant des établissements d'enseignement et de recherche français ou étrangers, des laboratoires publics ou privés.

Tracing isomanifolds in \mathbb{R}^d in time polynomial in d

Jean-Daniel Boissonnat

Université Côte d'Azur, Inria
[Sophia-Antipolis, France]
jean-daniel.boissonnat@inria.fr

Siargey Kachanovich

Université Côte d'Azur, Inria
[Sophia-Antipolis, France]
siargey.kachanovich@inria.fr

Mathijs Wintraecken

IST Austria
[Klosterneuburg, Austria]
m.h.m.j.wintraecken@gmail.com

1 — Abstract —

2 Isomanifolds are the generalization of isosurfaces to arbitrary dimension and codimension, i.e.
3 submanifolds of \mathbb{R}^d defined as the zero set of some multivariate multivalued smooth function
4 $f : \mathbb{R}^d \rightarrow \mathbb{R}^{d-n}$, where n is the intrinsic dimension of the manifold. A natural way to approximate
5 a smooth isomanifold \mathcal{M} is to consider its Piecewise-Linear (PL) approximation $\hat{\mathcal{M}}$ based on a
6 triangulation \mathcal{T} of the ambient space \mathbb{R}^d . In this paper, we describe a simple algorithm to trace
7 isomanifolds from a given starting point. The algorithm works for arbitrary dimensions n and d , and
8 any precision D . Our main result is that, when f (or \mathcal{M}) has bounded complexity, the complexity
9 of the algorithm is polynomial in d and $\delta = 1/D$ (and unavoidably exponential in n). Since it is
10 known that for $\delta = \Omega(d^{2.5})$, $\hat{\mathcal{M}}$ is $O(D^2)$ -close and isotopic to \mathcal{M} , our algorithm produces a faithful
11 PL-approximation of isomanifolds of bounded complexity in time polynomial in d . Combining
12 this algorithm with dimensionality reduction techniques, the dependency on d in the size of $\hat{\mathcal{M}}$
13 can be completely removed with high probability. We also show that the algorithm can handle
14 isomanifolds with boundary and, more generally, isostratifolds. The algorithm has been implemented
15 and experimental results are reported, showing that it is practical and can handle cases that are far
16 ahead of the state-of-the-art.

2012 ACM Subject Classification Theory of computation \rightarrow Computational geometry

Keywords and phrases Coxeter triangulation, Kuhn triangulation, permutahedron, PL-approximations, isomanifolds/solution manifolds/isosurfacing

Funding The research leading to these results has received funding from the European Research Council (ERC) under the European Union's Seventh Framework Programme (FP/2007-2013) / ERC Grant Agreement No. 339025 GUDHI (Algorithmic Foundations of Geometry Understanding in Higher Dimensions).

Jean-Daniel Boissonnat: Supported by the French government, through the 3IA Côte d'Azur Investments in the Future project managed by the National Research Agency (ANR) with the reference number ANR-19-P3IA-0002.

Mathijs Wintraecken: Supported by the European Union's Horizon 2020 research and innovation programme under the Marie Skłodowska-Curie grant agreement No. 754411.

Acknowledgements We thank Dominique Attali, Guilherme de Fonseca, Arijit Ghosh, Vincent Pilaud and Aurélien Alvarez for their comments and suggestions. We also acknowledge the reviewers.



© Jean-Daniel Boissonnat, Siargey Kachanovich, and Mathijs Wintraecken;
licensed under Creative Commons License CC-BY

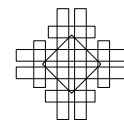
37th International Symposium on Computational Geometry (SoCG 2021).

Editors: TBA; Article No. ??; pp. ??:1–??:21



Leibniz International Proceedings in Informatics

LIPICs Schloss Dagstuhl – Leibniz-Zentrum für Informatik, Dagstuhl Publishing, Germany



17 **1 Introduction**

18 Given a surface represented in \mathbb{R}^3 as the zero set of a function $f : \mathbb{R}^3 \rightarrow \mathbb{R}$, the goal of
 19 isosurfacing is to find a piecewise linear (PL) approximation of the surface. This question
 20 naturally extends to isomanifolds of higher dimensions and codimensions defined as the zero
 21 set of multivariate multivalued smooth functions $f : \mathbb{R}^d \rightarrow \mathbb{R}^{d-n}$. Isosurfaces play a crucial
 22 role in medical imaging, computer graphics and geometry processing [24]. Higher dimensional
 23 isomanifolds are also of fundamental importance in many fields like statistics [11], dynamical
 24 systems [27], econometrics, or mechanics [24].

25 **State-of-the-art.** The most widely used algorithm to trace isomanifolds is the Marching
 26 Cube (MC) algorithm and its numerous variants [19, 29]. The MC algorithm uses a cubical
 27 grid to tessellate the ambient space. In many applications in 3-dimensions, the ambient space
 28 is decomposed into unstructured tetrahedral meshes, which led to the development of a
 29 variant of the MC algorithm named the Marching Tetrahedra algorithm. In higher dimensions,
 30 any tessellation of the ambient space has a complexity that depends exponentially on the
 31 ambient dimension. Hence a key to extending marching algorithms to higher dimensions is
 32 to circumvent the curse of dimensionality by using an *implicit* representation of the ambient
 33 tessellation. This is impossible for general triangulations but easy to do if one uses a grid.
 34 However, using a grid has other drawbacks and is not sufficient to break the exponential
 35 barrier. The reason for this is that the number of configurations inside a cubical cell
 36 grows exponentially with the dimension [29]. Hence the most promising approach seems to
 37 subdivide the ambient space \mathbb{R}^d using a highly regular triangulation such as the Freudenthal-
 38 Kuhn triangulation. Some early work along this direction has been published in Applied
 39 Mathematics [2, 17, 27], and a slightly more recent paper by Dobkin et al. [15] attracted the
 40 interest of the Computer Graphics community to the related Coxeter triangulations. Dobkin
 41 et al. however only considered the case of curves ($n = 1$). The most advanced work we are
 42 aware of is due to Min [23]. Min’s method uses the Freudenthal-Kuhn triangulation over
 43 a dyadic grid of \mathbb{R}^d and applies to isomanifolds of any dimension and codimension. The
 44 complexity of Min’s method is, with our notations, $O(\delta^m \log \delta)$, where $\delta = 1/D$ and D is the
 45 maximal diameter of the simplices. The ambient dimension d is a constant hidden in the
 46 big O . The fact that the exponent of δ is the intrinsic dimension m , and not the ambient
 47 dimension d is a clear improvement over earlier methods. However, although not explicitly
 48 analysed by Min, the complexity in d remains exponential, and the method seems limited to
 49 small ambient dimensions. Experimental results are only reported in dimensions 3, and 4.

50 **Contributions.** This paper discusses an efficient algorithm to compute a PL-approximation
 51 of isomanifolds. We extend the work of Dobkin et al. [15] and describe a simple
 52 algorithm to trace an n -dimensional isomanifold \mathcal{M} of \mathbb{R}^d for arbitrary n and d . Our
 53 algorithm uses any triangulation of a family of regular triangulations of \mathbb{R}^d that includes
 54 the Coxeter and the Freudenthal-Kuhn triangulations. Contrary to Min [23], our results are
 55 obtained with a uniform triangulation leading to a very simple algorithm. Key to our results,
 56 is a recently developed data structure that can implicitly store the full facial structure of
 57 such triangulations. As shown in [9] and recalled in Section 2.1, the data structure is very
 58 compact and allows to retrieve the faces or the cofaces of a simplex of any dimension in an
 59 output sensitive way. Using this data structure, one can trace a connected submanifold of
 60 \mathbb{R}^d , starting from a given initial point on the manifold (Section 3). Our algorithm produces a
 61 PL-approximation of size polynomial in d and $\delta = 1/D$, and exponential in n . The complexity
 62 of the algorithm is also polynomial in d , and δ , and exponential in n .

63 Moreover, by taking δ large enough, the PL-approximation output by the algorithm

64 is a faithful approximation of the isomanifold. Specifically, as shown in the full version
 65 of [10] and recalled in Section 2.2, if we take $\delta = \Omega(d^{2.5})$, the PL-approximation $\hat{\mathcal{M}}$ is
 66 $O(D^2)$ -close and isotopic to the isomanifold. Here the constants in the O depend on f and
 67 its derivatives. Hence, our algorithm constructs geometrically close and topologically correct
 68 PL-approximation of isomanifolds of bounded complexity in polynomial time.

69 Our algorithm can be extended in several directions. First, the dependency on d in
 70 the size of $\hat{\mathcal{M}}$ can be completely removed by combining our algorithm with dimensionality
 71 reduction (Section 3.4). We can also extend the algorithm to the case of isomanifolds with
 72 boundary and, more generally, to stratifolds (Section 3.5).

73 The algorithm has been implemented. In Section 4, we report on experimental results
 74 which show that the algorithm is practical and can handle cases that are far 16 ahead of the
 75 state-of-the-art. We also present an application in Algebraic Geometry that was used to verify
 76 a conjecture on projective varieties defined by polynomial equations in the complex projective
 77 plane. Following numerous experiments on various projective varieties, the conjecture was
 78 ultimately proved by Alvarez and Deroin [4].

79 The approximation of a manifold that is the zero set of a function is an example of the more
 80 general question of how to triangulate a manifold which has a long history in Mathematics.
 81 In particular, Whitney [30] introduced a construction that has some similarity with the
 82 present algorithm (see [7]). A major difference though is that topological guarantees can
 83 only be obtained if some intricate perturbations of the ambient triangulation are performed
 84 (Section 5). These techniques are at the moment incompatible with polynomial complexity.

85 **2 Background**

86 **2.1 Permutahedral representation of CFK-triangulations**

87 In this section, we recall the definitions and basic properties of Freudenthal-Kuhn and Coxeter
 88 triangulations. We also briefly describe a compact data structure to store such triangulations
 89 which is fully described in [8].

90 Both triangulations can be described as an arrangement of hyperplanes. They are identical
 91 under an affine map. Let E be a finite set of vectors of \mathbb{R}^d and consider the set of hyperplanes
 92 $H_E = \{x \in \mathbb{R}^d \mid \langle x, u \rangle = k, u \in E, k \in \mathbb{Z}\}$. Let, in addition, H be the hyperplane of \mathbb{R}^{d+1} of
 93 equation $\langle x, \mathbf{1} \rangle = 0$ where $\mathbf{1}$ is the vector of \mathbb{R}^{d+1} whose coordinates are all 1.

94 **► Definition 1.** *The Freudenthal-Kuhn triangulation is the hyperplane arrangement \mathcal{H}_{FK}*
 95 *associated to the set of vectors $E_{FK} = \{e_1, \dots, e_d\} \cup \{u_{i,j} = e_j - e_i \mid 1 \leq i < j \leq d\}$.*

96 *The Coxeter triangulation of type \tilde{A}_d is the hyperplane arrangement \mathcal{H}_{EC} in \mathbb{R}^{d+1} asso-*
 97 *ciated to the set of vectors $E_C = \{r_{i,j} = e_i - e_{j+1} \mid 1 \leq i \leq j \leq d\}$, restricted to $H \simeq \mathbb{R}^d$.*

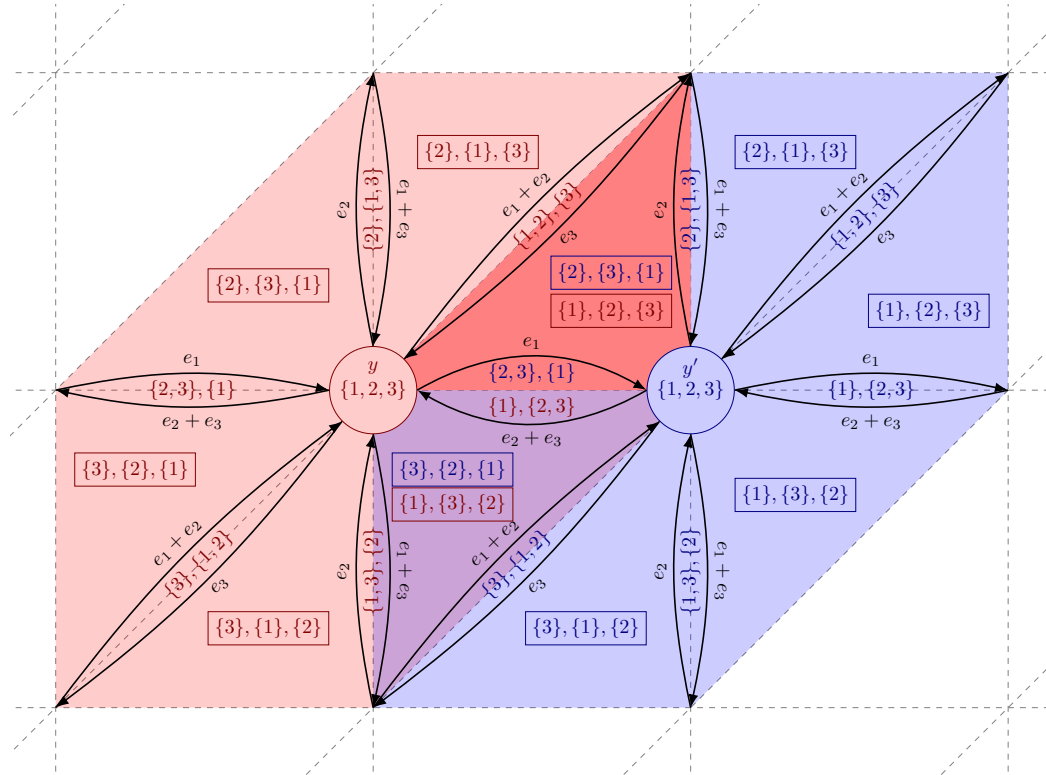
98 Two important facts follows. On one hand, Coxeter and Freudenthal-Kuhn triangulations
 99 are related by an affine transformation and have thus the same combinatorial structure. We
 100 call any triangulation that is the image of a Freudenthal-Kuhn triangulation under an affine
 101 transformation a CFK-triangulation. In this paper, we restrict our attention to Coxeter and
 102 Freudenthal triangulations since they are the most important but any CFK-triangulation
 103 could be used.

104 The second fact is that each simplex in such a triangulation can be represented as a cell
 105 in an arrangement of $d(d-1)/2$ hyperplanes which are known and do not need to be stored.

106 The next crucial observation relates CFK-triangulations and permutahedra, which allows
 107 to represent CFK-triangulations in a compact way (The definition and some combinatorial
 108 properties of permutahedra are given in Appendix A).

110 ► **Proposition 2.** *The star of a vertex in a CFK-triangulation is dual¹ to a permutahedron*
 111 *(combinatorially).*

112 Since the facial structure of a permutahedron is fully described by ordered partitions,
 113 any simplex σ in a CFK-triangulation is characterized by a star that contains σ and by the
 114 ordered partition that specifies which simplex in the star is precisely σ . Since a simplex
 115 appears in several stars, we take the one that is centered at the lowest vertex of σ in the
 116 lexicographic order. This representation is called the permutahedral representation of a
 117 CFK-triangulation. See Figure 1 from [8] for an illustration.



118 ■ **Figure 1** The permutahedral representation of the simplices in the stars of vertices y and y' .

119 The following results are given in [8]

120 ► **Lemma 3** (Face computation). *Let σ be an l -simplex in the FK-triangulation of \mathbb{R}^d .*
 121 *Computing all its k -faces can be done in time $O(ds)$, where $s = \binom{l+1}{k+1}$ is the number of*
 122 *k -faces of an l simplex. The space complexity of the algorithm is $O(l)$.*

123 ► **Lemma 4** (Coface computation). *Let σ be a k -simplex in the FK-triangulation of \mathbb{R}^d given*
 124 *by its permutahedral representation. Computing the permutahedral representations of all its*
 125 *l -cofaces can be done in time $O(ds)$, where $s \leq \frac{1}{2^{\min(l,d-l)}} \binom{d-k}{d-l} (d-k+1)!$ is the number of*
 126 *l -cofaces of a k -simplex in the FK-triangulation. The space complexity of the algorithm is*
 127 *$O(d)$.*

109 ¹ Two complexes are dual if there is a bijection between their faces that inverses the inclusion relationships.

128 Although all CFK-triangulations have the same combinatorial structure, they geometric
 129 properties are different (this point will be further discussed in Section 3.3).

130 **2.2 PL-approximation of isomanifolds**

131 We first recall sufficient conditions under which the PL-approximation $\hat{\mathcal{M}}$ output by the
 132 algorithm faithfully reproduces the original isomanifold. These conditions are fully described
 133 in the full version of [10] and we simply state here the main results specialized to the case of
 134 CFK-triangulations.

135 We will say that f has *bounded complexity* if the three following quantities γ_{\max} , λ_{\min}
 136 and α_{\max} are positive and bounded.

$$137 \quad \gamma_{\max} = \max_{x \in \mathcal{T}_0} (\max_i |\text{grad} f^i(x)|)$$

$$138 \quad \lambda_{\min} = \min_{x \in \mathcal{T}_0} \lambda_{\min}(x),$$

$$139 \quad \alpha_{\max} = \max_{x \in \mathcal{T}_0} \max_i \|\text{Hes}(f^i)(x)\|_2$$

140 where

- 141 ■ \mathcal{T}_0 denotes the set of all $\sigma \in \mathcal{T}$, such that $(f^i)^{-1}(0) \cap \sigma \neq \emptyset$ for all i .
- 142 ■ $\text{grad} f^i = (\partial_j f^i)_j$ denotes the gradient of component f^i , for $i \in [1, d - n]$,
- 143 ■ $\text{Gram}(\nabla f)$ denotes the Gram matrix whose elements are $\nabla f^i \cdot \nabla f^j$ where \cdot stands for
 144 the dot product.
- 146 ■ $\lambda_{\min}(x)$ denotes the smallest absolute value of the eigenvalues of $\text{Gram}(\nabla f(x))$,²
- 147 ■ $\text{Hes}(f) = (\partial_k \partial_l f^i)_{k,l}$ denotes the Hessian matrix of second order derivatives,
- 149 ■ $|\cdot|$ denotes the Euclidean norm of a vector and $\|\cdot\|_2$ the operator 2-norm of a matrix.³

150 We can now restate the topological result of [10] :

151 ► **Theorem 5.** *Assume that the function f has bounded complexity. If the precision of the*
 152 *CFK-triangulation satisfies $D = O(d^{-5/2})$, where the constant in the big O depends on γ_{\max} ,*
 153 *λ_{\min} and α_{\max} , then $\hat{\mathcal{M}}$ is a manifold isotopic to the zero set \mathcal{M} of f .*

154 Moreover, we can bound the Fréchet distance between \mathcal{M} and $\hat{\mathcal{M}}$. The Fréchet distance
 155 is a quite strong notion of distance and, in particular, it bounds the Hausdorff distance.

156 ► **Definition 6** (Fréchet distance for embedded manifolds). *Let \mathcal{M}_a and \mathcal{M}_b be two homeo-*
 157 *morphic, compact submanifolds of \mathbb{R}^d . Write \mathcal{H} for the set of all homeomorphisms from \mathcal{M}_a*
 158 *to \mathcal{M}_b . The Fréchet distance between \mathcal{M}_a and \mathcal{M}_b is*

$$159 \quad d_F(\mathcal{M}_a, \mathcal{M}_b) = \inf_{h \in \mathcal{H}} \sup_{x \in \mathcal{M}_a} d(x, h(x)).$$

160 We can now state the other main result of [10]:

161 ► **Theorem 7.** *Assume that the function f has bounded complexity. Then, $d_F(\mathcal{M}, \hat{\mathcal{M}}) =$*
 162 *$O(D^2)$ where the constant in the big O depends on γ_{\max} , λ_{\min} and α_{\max} .*

145 ² Because a Gram matrix is a symmetric square matrix, its eigenvalues are well defined and real.

148 ³ The operator norm is defined as $\|A\|_p = \max_{x \in \mathbb{R}^n} \frac{|Ax|_p}{|x|_p}$, with $|\cdot|_p$ the p -norm on \mathbb{R}^n .

163 **3 Tracing isomanifolds**

164 In this section, we describe an algorithm that computes a PL-approximation $\hat{\mathcal{M}}$ of an
 165 isomanifold \mathcal{M} . The algorithm has some similarity with the Marching Cube algorithm [22]
 166 but departs from it in two fundamental ways. First, because of the curse of dimensionality,
 167 we cannot afford to look at all the cells in the grid and need to limit the search to cells
 168 that are close to \mathcal{M} . The problem of computing $\hat{\mathcal{M}}$ can be naturally decomposed into two
 169 subproblems: locating the various components of \mathcal{M} (i.e., finding at least one point in each
 170 component), and then tracing around each component, using the fact that the components
 171 are connected. This decomposition is used by various authors, see for example [29, 15]. In
 172 this paper, we focus on the tracing problem, although we discuss very briefly (Section 3.2)
 173 the problem of locating the components. As pointed out by Dobkin et al. many applications
 174 supply their own starting points.

175 The second major difference with the original marching cube algorithm is to replace the
 176 usual cubical grid by a CFK-triangulation of the ambient space. Taking a CFK-triangulation
 177 instead of a grid is a major advantage in high dimensions that has been recognized in the
 178 pioneering works of Allgower, and Schmidt [3] and of Dobkin et al. [15], see also [23]. The
 179 novelty here is to use the data structure of Section 2.1 to represent a CFK-triangulation. As
 180 a consequence, we will keep two main advantages of using grids: very limited storage and
 181 fast basic operations.

182 **3.1 Isomanifolds**

183 Let $f : \mathbb{R}^d \rightarrow \mathbb{R}^{d-n}$ be a smooth (C^2 suffices) function, and suppose that 0 is a regular value
 184 of f , meaning that at every point x such that $f(x) = 0$, the Jacobian of f is non-degenerate.
 185 Then the zero set of f is an n -dimensional manifold as a direct consequence of the implicit
 186 function theorem, see for example [16, Section 3.5]. We further assume that $f^{-1}(0)$ is compact.
 187 As in [1] we consider a triangulation \mathcal{T} of \mathbb{R}^d . The function \hat{f} is the linear interpolation of
 188 the values of f at the vertices if restricted to a single simplex $\sigma \in \mathcal{T}$, i.e.

189
$$\forall x \in \sigma : \hat{f}(x) = \sum_{v \in \sigma} \lambda_v(x) f(v), \tag{1}$$

190 where the λ_v are the barycentric coordinates of x with respect to the vertices of σ . For any
 191 function $g : \mathbb{R}^d \rightarrow \mathbb{R}^{d-n}$ we write g^i , with $i = 1, \dots, d-n$, for the components of g .

192 The PL-approximation is now defined as $\hat{f}^{-1}(0) = \hat{\mathcal{M}}$. Locally, $\hat{f}|_{\sigma}^{-1}(0)$ is generically
 193 the intersection of an n -flat H_{σ} with σ . More precisely we note that $\hat{f}|_{\sigma}^{-1}(0)$ is an n -flat if
 194 the gradients of $\hat{f}^i|_{\sigma}$ are linearly independent, which can be easily achieved by perturbing f
 195 infinitesimally (or at least its values at the vertices). Let τ_i^{d-n} and τ_i^{d-n-1} be faces of σ of
 196 dimension $d-n$ and $d-n-1$. An infinitesimal perturbation of f , can prevent either $\hat{f}|_{\sigma}^{-1}(0)$
 197 from intersecting the faces τ_i^{d-n-1} , or the gradients of $\hat{f}^i|_{\sigma}$ and the normal spaces of τ_i^{d-n}
 198 (for each fixed i) from failing to span \mathbb{R}^d . More precise statements on the geometric and
 199 topological stability of the triangulation under perturbations of f can be found in the full
 200 version of [10, Section 5]. Because $\hat{f}|_{\sigma}^{-1}(0)$ is (generically) the intersection of an n -flat (H_{σ})
 201 and σ , it is an n -dimensional polytope denoted by C_{σ} . The PL-approximation or mesh $\hat{\mathcal{M}}$
 202 of \mathcal{M} is the polytopal cell complex obtained by gluing the polytopes C_{σ} associated to all the
 203 simplices σ in \mathcal{T} .

204 **3.2 Manifold tracing algorithm**

205 Let \mathcal{M} be the zero set of some function $f : \mathbb{R}^d \rightarrow \mathbb{R}^{d-n}$, and let $\hat{\mathcal{M}}$ be the associated
 206 PL-approximation defined over a triangulation \mathcal{T} of the ambient space \mathbb{R}^d . Both n , and d are
 207 known but arbitrary, and will be considered as parameters in the complexity analysis. We
 208 write $k = d - n$ for the codimension of \mathcal{M} . The algorithm will use for \mathcal{T} a CFK-triangulation
 209 stored using the data structure from Section 2.1. We assume that the manifold $\hat{\mathcal{M}}$, and the
 210 triangulation \mathcal{T} satisfy the following genericity hypothesis:

211 ► **Hypothesis 8 (Genericity).** *Let σ be a d -simplex of \mathcal{T} that intersects H_σ . No subface of σ
 212 of dimension less than k intersects H_σ , and any subface of σ of dimension k intersects H_σ
 213 in at most one point and transversally.*

214 We note that this condition can be satisfied by an infinitesimal perturbation for isomani-
 215 folds. This requires some explanation. We recall that the CFK-triangulation is a hyperplane
 216 arrangement, and up to translation there are a finite number of k -flats that contain all
 217 k -simplices in the CFK triangulation. Hypothesis 8 is not satisfied, if either the flat H_σ
 218 is not linearly independent of these k -flats, or if H_σ does intersect some $(k - 1)$ -flat in
 219 the CFK-triangulation. In the previous section, we have already seen that an infinitesimal
 220 perturbation ensures that H_σ is n -dimensional. Because two affine spaces whose dimensions
 221 do not add up to the ambient dimension don't intersect with genericity and two affine spaces
 222 whose dimensions add up to exactly the ambient dimension intersect in a single point, we see
 223 that genericity can be achieved by perturbing f infinitesimally. refer to We further remark
 224 that, generically, any vertex of the PL-approximation $\hat{\mathcal{M}}$ is the intersection point between a
 225 k -simplex σ of \mathcal{T} with the n -flat H_σ that interpolates f inside σ .

226 ■ **Algorithm 1** Manifold tracing algorithm

```

226 input : the permutahedral representation of a triangulation  $\mathcal{T}$  of  $\mathbb{R}^d$ ,
227         the codimension of the isomanifold  $k = d - n$ ,
228         a seed  $k$ -simplex  $\tau_0$  that intersects  $\hat{\mathcal{M}}$ 
229 oracle : Given a  $k$ -simplex  $\sigma$  of  $\mathcal{T}$ , decide whether  $\sigma$  intersects  $H_\sigma$  and, in the
           affirmative, report the corresponding vertex  $\sigma \cap H_\sigma = \sigma \cap \hat{\mathcal{M}}$ .
230 output : Set  $\mathcal{S}$  of the simplices in  $\mathcal{T}$  of dimension  $k$  that intersect  $\hat{\mathcal{M}}$ , represented by
           their permutahedral representation, and the corresponding set  $\hat{\mathcal{M}}_0$  of
           intersection points
231 Initialize the queue  $\mathcal{Q}$  and the set  $\mathcal{S}$  with  $\tau_0$ 
232 while the queue  $\mathcal{Q}$  is not empty do
233     Pop a  $k$ -dimensional simplex  $\tau$  from  $\mathcal{Q}$ 
234     foreach cofacet  $\phi$  of  $\tau$  do
235         foreach facet  $\sigma$  of  $\phi$  do
236             if  $\sigma$  does not lie in  $\mathcal{S}$  and intersects  $\hat{\mathcal{M}}$  (which can be decided using the
                oracle) then
237                 Insert  $\sigma$  in the queue  $\mathcal{Q}$ 
238                 Insert  $\sigma$  together with the intersection point in  $\mathcal{S}$  provided by the oracle
    
```

227 The algorithm essentially computes the set \mathcal{S} of k -simplices of \mathcal{T} that intersect $\hat{\mathcal{M}}$. The
 228 elements of \mathcal{S} which are in 1-1 correspondence with the vertices of $\hat{\mathcal{M}}$ thanks to the Genericity
 229 hypothesis. The so-called intersection oracle is a basic ingredient of the algorithm:

230 **Intersection oracle:** *Given a k -simplex σ of \mathcal{T} , decide whether σ intersects H_σ and, in*
 231 *the affirmative, report the corresponding vertex $\sigma \cap H_\sigma$.*

232 It is easy to see that the intersection oracle reduces to solving a linear system. Indeed,
 233 generically, a vertex is the intersection of a k -simplex σ of \mathcal{T} with the m -flat H_σ that
 234 interpolates f inside σ . One can compute the barycentric coordinates of $\sigma \cap H_\sigma$ by solving
 235 a linear system of k equations, and k unknowns. It then remains to check whether the
 236 barycentric coordinates are all non-negative (to ensure that the intersection point lies inside
 237 σ). It follows that the intersection oracle reduces to evaluating f at the $k + 1$ vertices of σ
 238 plus solving a $k \times k$ linear system.

239 In addition, we need to provide a set of k -simplices of \mathcal{T} to initialize the tracing. These
 240 simplices must intersect all the connected components of the isomanifold and are called
 241 seed simplices. If \mathcal{M} consists of multiple connected components, then a seed simplex must
 242 be provided per each connected component and we proceed in the same manner for each
 243 component. So we will assume for now that \mathcal{M} is connected.

244 The seed simplices are given as part of the input and we don't discuss in this paper the
 245 problem of their construction. We simply observe that they can be obtained by computing a
 246 critical point (e.g., a point with smallest x_1 -coordinate) on each connected component of the
 247 isomanifold, which reduces to finding a solution to a system of equations, on which a large
 248 body of literature exists. See for example [26, 25, 15] and also the discussion in Wenger's
 249 book [29, Section 8.4]. Once such a seed point has been computed, we simply translate
 250 and rotate the triangulation \mathcal{T} so that the seed point coincides with the barycenter of a
 251 k -simplex of \mathcal{T} and the intersection with the manifold is transversal as demanded by the
 252 genericity hypothesis (for numerical stability it is convenient if the angle between the tangent
 253 space of the manifold and the starting k -simplex is large, which is easy to ensure). If the
 254 distance between \mathcal{M} and $\hat{\mathcal{M}}$ is small enough, then $\hat{\mathcal{M}}$ also intersects the same k simplex, see
 255 Section 2.2.

256 The algorithm is described as Algorithm 1. It takes as input the permutahedral represen-
 257 tation of an ambient FKC-triangulation \mathcal{T} and a seed k -simplex τ_0 of \mathcal{T} . We assume that \mathcal{T}
 258 satisfies the Genericity Hypothesis 8, which can be enforced by infinitesimal perturbations of
 259 f as discussed in Section 3.1.

260 The algorithm maintains the subset \mathcal{S} of the simplices in \mathcal{T} of dimension k that intersect
 261 $\hat{\mathcal{M}}$. \mathcal{S} is initialized with the seed simplex τ_0 and stored as a hash table so that we can decide
 262 in constant time if a given k -simplex belongs to \mathcal{S} . Then, starting from τ_0 , we look at all its
 263 cofacets and consider all the facets of those cofacets that are not in \mathcal{S} (i.e. they have not
 264 been considered yet). This can be done using a queue \mathcal{Q} of candidate k -simplices. Each of
 265 these simplices is queried with the intersection oracle and, if it is found to intersect $\hat{\mathcal{M}}$, it
 266 is added to \mathcal{S} if not already present. Upon termination, \mathcal{S} contains all the k -dimensional
 267 simplices of \mathcal{T} that intersect $\hat{\mathcal{M}}$. Each such intersection, which consists of a single point (by
 268 the Genericity hypothesis), is a vertex of $\hat{\mathcal{M}}$. Hence $\hat{\mathcal{M}}_0$ is the vertex set of $\hat{\mathcal{M}}$.

269 Note that our algorithm essentially traverses the adjacency graph of the k and $(k + 1)$ -
 270 simplices of \mathcal{T} that intersect $\hat{\mathcal{M}}$. It therefore identifies not only the set $\hat{\mathcal{M}}_0$ of vertices of $\hat{\mathcal{M}}$,
 271 but also the edges joining two such vertices (associated to the cofacets of the k -simplices in
 272 \mathcal{S}). By simply reporting those cofacets on the fly, the algorithm can output the 1-skeleton
 273 $\hat{\mathcal{M}}_1$ of the n -dimensional polytopal cell complex $\hat{\mathcal{M}}$. The higher dimensional faces of $\hat{\mathcal{M}}$ are
 274 the polytopes $C_\tau = \tau \cap H_\tau$ for all the cofaces τ of the k -simplices of \mathcal{S} . If needed, the full
 275 Hasse diagram of $\hat{\mathcal{M}}$ can be computed from $\hat{\mathcal{M}}_0$. This can be done in an output sensitive
 276 manner by using the permutahedral representation of \mathcal{T} and the algorithm of Section 2.1 to
 277 compute cofaces by increasing dimensions.

278 **3.3 Complexity analysis**

279 We can easily bound the complexity of the manifold tracing algorithm as a function of the
280 size of the output.

281 ► **Proposition 9.** *The time complexity of the algorithm is $O(k2^n I|\mathcal{S}|)$ where I is the time
282 complexity of one call of the intersection oracle, and $|\mathcal{S}|$ is the number of simplices of
283 dimension k output by the algorithm.*

284 Since, the intersection oracle reduces to evaluating f at the $k + 1$ vertices of σ plus solving
285 a $k \times k$ linear system, $I = O(k^\omega)$ where $\omega \approx 2.375$.

286 We will now express the size of the output in terms of quantities that depend on the
287 manifold, the ambient dimension d , and the resolution of the triangulation (the diameter
288 D of a simplex) which bounds the density of the output sample, and the precision of the
289 approximation. Our result holds for K -sparse manifolds, i.e. submanifolds whose intersection
290 with any k -flat consists of at most K points. In practical situations, K is usually small and,
291 in particular, K is a constant for algebraic isomanifolds of bounded degree.

292 ► **Proposition 10 (Size of the output).** *Assume that \mathcal{M} is contained in the unit cube $C_d =$
293 $[0, 1]^d$, and that any k -flat intersects \mathcal{M} at most K times. Writing $|\mathcal{S}| = N_C$ when \mathcal{T} is
294 a Coxeter triangulation and $|\mathcal{S}| = N_{FK}$ for a Freudenthal triangulation, we have $N_C \leq$
295 $\frac{K}{n!} \times \left(\frac{d^2 \sqrt{d(d+2)}}{2\sqrt{2}D}\right)^n$ and $N_{FK} \leq \frac{K}{n!} \times \left(\frac{d^3}{\sqrt{2}D}\right)^n$ where D is the diameter of a simplex of \mathcal{T} .*

296 We see that Coxeter triangulations lead to smaller samples than FK-triangulations by a
297 factor of roughly 2^n . This will be confirmed experimentally (see Figure 3).

298 As noticed in Section 3.2, a simple variant of the algorithm can compute the full Hasse dia-
299 gram of $\hat{\mathcal{M}}$ in an output sensitive manner. The following lemma shows that the combinatorial
300 complexity of $\hat{\mathcal{M}}$ is of the same order as the combinatorial complexity as $\hat{\mathcal{M}}_0$.

301 ► **Proposition 11.** *The combinatorial complexity of $\hat{\mathcal{M}}$ is $|\mathcal{S}| \times (\frac{3}{2})^n (n + 1)!$, where $|\mathcal{S}|$ is
302 bounded in Proposition 10. If $n = O(1)$, the combinatorial complexity of $\hat{\mathcal{M}}$ is polynomial in
303 d , and $\delta = 1/D$.*

304 We combine Propositions 9, 10, and 11 to obtain our main result.

305 ► **Theorem 12.** *Assume that \mathcal{M} is contained in the unit cube $[0, 1]^d$ and that any affine
306 k -flat intersects \mathcal{M} at most K times (K is usually small, and is in particular a constant for
307 algebraic isomanifolds of bounded degree). Let, in addition, D be the precision required on the
308 approximation (the diameter of a simplex in the ambient triangulation \mathcal{T}). The size of the
309 output, and the time complexity of the algorithm are polynomial in the ambient dimension d ,
310 and in $\delta = 1/D$, and exponential in the intrinsic dimension n . The same result holds for the
311 full PL-approximation $\hat{\mathcal{M}}$ of \mathcal{M} .*

312 **3.4 Dimensionality reduction**

313 As seen from Proposition 10, the size $|\mathcal{S}|$ of the output of the algorithm, considered as a
314 function of the resolution D of the triangulation, depends exponentially on n (which is to be
315 expected), and only polynomially on d (which is fortunate). Nevertheless, the computing
316 time of our algorithm and the size of the output depend on d . Removing the dependency on
317 d in the time complexity is impossible since we need to evaluate a vectored-valued function
318 f at a number of points of \mathbb{R}^d , which takes $\Omega(d)$ time per evaluation. However, we will see
319 that we can reduce the size of the mesh produced by our algorithm.

320 Examples of samples of \mathcal{M} whose sizes depend on n but not on d , and lead to good
 321 approximations are known. Especially important are D -nets [12, 6]. A D -net consists of
 322 a finite number of sample points of \mathcal{M} such that no point of \mathcal{M} is at distance more than
 323 D from a sample point (density condition), and no two sample points are closer than cD
 324 for some positive constant c (separation condition). A simple volume argument shows that
 325 the size of a D -net of a n -dimensional smooth submanifolds is $O(1/D^n)$ [5, Lemma 5.3].
 326 The sample produced by our algorithm is D -dense on the piecewise linear approximation.
 327 This implies that we have a sample that has a Hausdorff distance of $D + d_F(\mathcal{M}, \hat{\mathcal{M}})$ to the
 328 manifold, where $d_F(\mathcal{M}, \hat{\mathcal{M}})$ is bounded in Theorem 7.

329 Since its cardinality depends on d , it is not well separated and, in particular, not a D -net
 330 of \mathcal{M} . If we are mostly interested in the output sample, we can easily sparsify it to obtain a
 331 D -net. However, by doing so, we will lose the combinatorial structure of the mesh.

332 We now show how to compute a D -dense sample of \mathcal{M} of size independent of d , together
 333 with a mesh. Specifically, we will reduce dimensionality using a variant of the celebrated
 334 Johnson-Lindenstrauss lemma for manifolds. Doing so, we depart from our previous worst-
 335 case analysis by allowing some approximation factor ε and tolerate a guarantee that holds
 336 only with high probability.

337 ► **Theorem 13** (Johnson-Lindenstrauss lemma for manifolds [14, 28])). *Pick any $\varepsilon, \eta > 0$,*
 338 *and let $d' = \Omega\left(\frac{n}{\varepsilon^2} \log \frac{1}{\varepsilon} + \frac{1}{\varepsilon^2} \log \frac{\Gamma}{\eta}\right)$, where Γ is a quantity that depends only on intrinsic*
 339 *properties of \mathcal{M} . Let Φ be the projection on a random affine subspace of dimension d' . Then,*
 340 *with probability $> 1 - \eta$, for all $x, y \in \mathcal{M}$, we have $(1 - \varepsilon) \sqrt{\frac{d'}{d}} \leq \frac{\|\Phi x - \Phi y\|}{\|x - y\|} \leq (1 + \varepsilon) \sqrt{\frac{d'}{d}}$.*

341 Let $\Psi = \sqrt{\frac{d}{d'}} \Phi$. By the theorem, the image $\Psi(\mathcal{M})$ of \mathcal{M} is a submanifold of dimension n
 342 embedded in $\mathbb{R}^{d'}$. One can now run the manifold tracing algorithm in $\mathbb{R}^{d'}$ to sample, and
 343 mesh $\Psi(\mathcal{M})$. The algorithm works as described before except that we need another oracle
 344 that, given a $(d' - n)$ -simplex σ of the CFK-triangulation of $\mathbb{R}^{d'}$, decides whether its inverse
 345 image $\Psi^{-1}(\sigma)$ intersects \mathcal{M} or not. Note that $\Psi^{-1}(\sigma)$ is a $(d - d')$ -dimensional flat strip
 346 (that is the product of a face and an affine subspace) in \mathbb{R}^d , and that the complexity of this
 347 new oracle is the same as the complexity of the basic intersection oracle, i.e. polynomial in d .

348 Due to the scaling factor $\sqrt{d/d'}$, the resolution of the triangulation in the low dimensional
 349 space $\mathbb{R}^{d'}$ has to be scaled by the same factor if one wants to satisfy a given sampling density
 350 on \mathcal{M} . Since the geometry of the manifold is also scaled in the same way [18], the analysis
 351 of the algorithm will be unchanged. Proposition 10 then shows that the size of the output
 352 sample does not depend on d but only on n and D for fixed ε , and η . Moreover, since the
 353 complexities of the projection and of the new oracle are polynomial in d , Proposition 9
 354 implies that the overall complexity is still polynomial in d .

355 3.5 Isomanifolds with boundary, and stratifolds

356 The case of isomanifolds with boundary and, more generally, of isostratifolds can be handled
 357 in very much the same way. By an isomanifold of dimension n with boundary, we mean that,
 358 on top of a function $f : \mathbb{R}^d \rightarrow \mathbb{R}^{d-n}$, we are given another function $f_\partial : \mathbb{R}^d \rightarrow \mathbb{R}$, and the set
 359 we consider is $\mathcal{M} = f^{-1}(0) \cap f_\partial^{-1}([0, \infty))$. We note that $\partial\mathcal{M} = f^{-1}(0) \cap f_\partial^{-1}(0)$.

360 Similarly to (1), we also define $\hat{f}_\partial|_\tau(x) = \sum_{i=1}^{j+1} \lambda_i(x) f_\partial(p_i)$. We write \hat{f} for the (global)
 361 piecewise linear function that coincides with $\hat{f}|_\tau$ on each τ of \mathcal{T} , and \hat{f}_∂ for the (global)
 362 piecewise linear function that coincides with $\hat{f}_\partial|_\tau$ on each τ of \mathcal{T} . We note that the piecewise
 363 linear approximation of the boundary $\partial\hat{\mathcal{M}} = \hat{f}_\partial^{-1}(0) \cap \hat{f}^{-1}(0)$ is a subset of $\hat{f}^{-1}(0)$, i.e. the

364 piecewise linear approximation of the manifold ignoring the boundary. The piecewise linear
 365 approximation $\hat{\mathcal{M}}$ of the manifold with boundary consists of the following cells:

- 366 ■ For each τ of \mathcal{T} , such that $\hat{f}_\partial|_\tau$ is positive on τ , and $(\hat{f}|_\tau)^{-1}(0) \cap \tau \neq \emptyset$, we add
 367 $(\hat{f}|_\tau)^{-1}(0) \cap \tau$.
- 368 ■ For each τ of \mathcal{T} , such that $(\hat{f}|_\tau)^{-1}(0) \cap \tau \neq \emptyset$, and $(\hat{f}_\partial|_\tau)^{-1}(0) \cap \tau \neq \emptyset$, we add
 369 $(\hat{f}|_\tau)^{-1}(0) \cap (\hat{f}_\partial|_\tau)^{-1}([0, \infty)) \cap \tau$.

370 We will assume that the Genericity Hypothesis 8 holds for both $\hat{\mathcal{M}}$, and $\partial\hat{\mathcal{M}}$.

371 We can now adapt the algorithm of Section 3.2 as follows. In addition to reporting the
 372 set S_k of k -faces of the triangulation \mathcal{T} that intersect $\hat{\mathcal{M}}$, the algorithm will also report the
 373 set S_{k+1} of $(k+1)$ -faces of the triangulation \mathcal{T} that intersect $\partial\hat{\mathcal{M}}$. The computation of S_{k+1}
 374 is done by the following simple modification of Lines 6-9: if the k -dimensional facet σ of τ
 375 intersects $\hat{f}^{-1}(0)$ at a point x such that $\hat{f}_\partial|_\tau(x) < 0$ (i.e. x is not in $\hat{\mathcal{M}}$), we then compute
 376 the intersection point of τ with $\hat{f}_\partial^{-1}(0)$, and put τ in S_{k+1} .

377 As for the case of manifolds without boundary (see the discussion at the end of Section 3.2),
 378 the algorithm traverses (and therefore computes) the 1-skeleton of $\hat{\mathcal{M}}$. Under the Genericity
 379 Hypothesis 8, the vertices of $\hat{\mathcal{M}}_1$ are in bijection with the simplices of $S_k \cup S_{k+1}$. The edges
 380 are obtained by applying the following rules below (we identify a simplex in S_k (resp. S_{k+1})
 381 and the intersection point $S_k \cap \hat{\mathcal{M}}$ (resp. $S_{k+1} \cap \partial\hat{\mathcal{M}}$):

- 382 1. Two simplices σ_1 , and σ_2 of S_k are joined by an edge in $\hat{\mathcal{M}}_1$ if and only if there exists a
 383 simplex in \mathcal{T}_{k+1} with faces σ_1 , and σ_2 .
- 384 2. Two simplices τ_1 , and τ_2 of S_{k+1} are joined by an edge in $\widehat{\partial\mathcal{M}}_1$ if and only if there exists
 385 a simplex in \mathcal{T}_{k+2} with faces τ_1 , and τ_2 .
- 386 3. A simplex σ of S_k , and a simplex τ of S_{k+1} are joined by an edge in $\widehat{\partial\mathcal{M}}_1$ if and only if
 387 σ is a facet of τ .

388 The three rules above together with the permutahedral representation of \mathcal{T} provide a way
 389 to construct the 1-skeleton of $\hat{\mathcal{M}}$ on the fly. The total cost is output sensitive. If needed, the
 390 entire combinatorial structure of $\hat{\mathcal{M}}$ can be computed by traversing the full triangulation \mathcal{T} .

391 The above construction generalizes easily to arbitrary isostratifolds. Isostratifolds are
 392 stratifolds that are defined by equations, and inequalities. An example of such a stratifold is
 393 an octant of the sphere in \mathbb{R}^3 that can be defined by as $x^2 + y^2 + z^2 - 1 = 0$, $x \geq 0$, $y \geq 0$,
 394 and $z \geq 0$. We compute the 1-skeleton of $\hat{\mathcal{M}}$, and construct a graph whose nodes are the
 395 simplices of dimensions $k, k+1, \dots, d$ that intersect the strata of dimension $n, n-1, \dots, 0$.

396 4 Experimental results

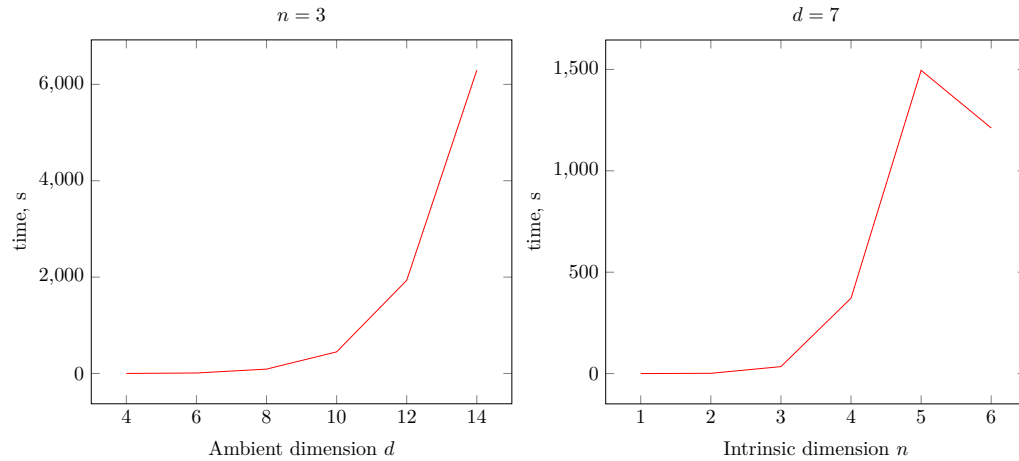
397 The data structure of Section 2.1 and the algorithm of Section 3 have been implemented in
 398 C++. The code is robust and fast and will be released in the GUDHI library [20]. Full detail
 399 on the implementation, including the implementation of the oracle, can be found in [21].

400 In this section, we explore the dependency of our C++ implementation of the data structure
 401 for the ambient CFK-triangulation, and of the manifold tracing algorithm on the properties
 402 of the triangulation, and of the input manifold.

403 4.1 Performance of the algorithm

404 We show the performance of our implementation of the manifold tracing algorithm for
 405 various ambient and intrinsic dimensions in Figure 2. In Figure 3, we can see that using

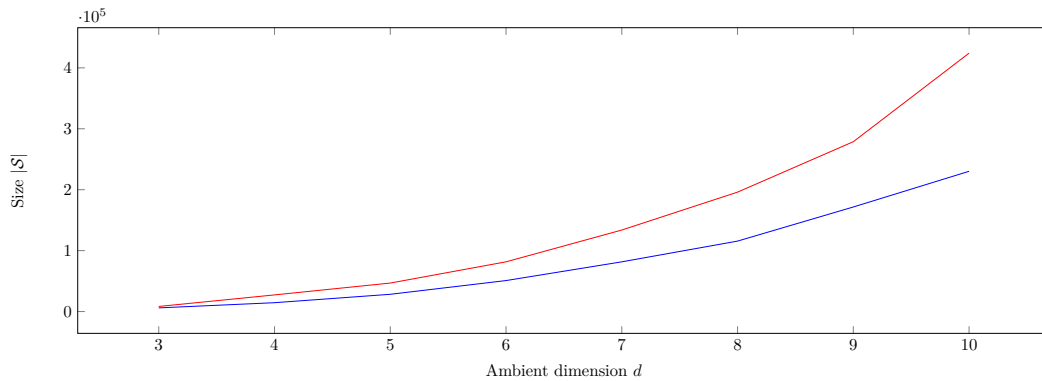
??:12 Tracing isomanifolds in \mathbb{R}^d in time polynomial in d



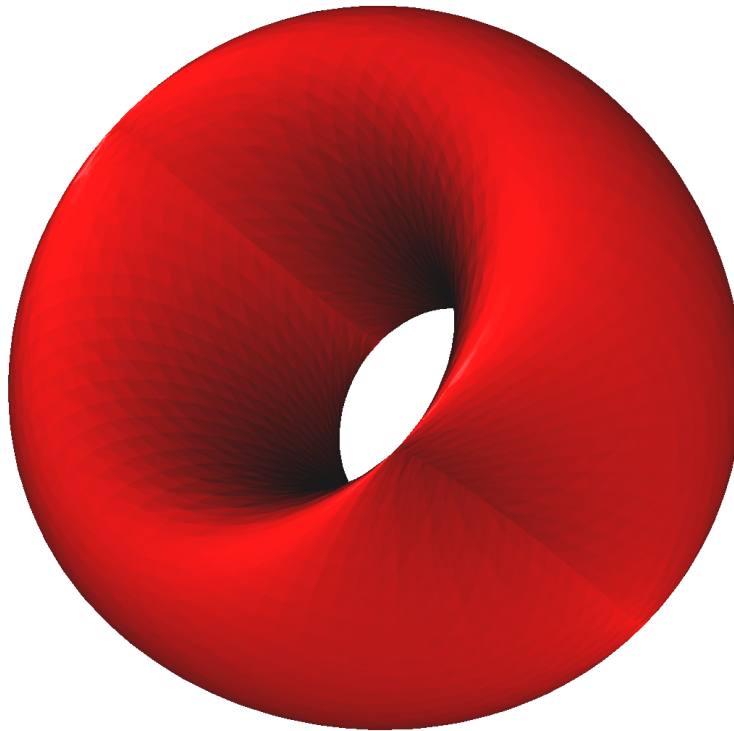
408 **Figure 2** The effect of the ambient dimension d and of the intrinsic dimension n on the computation
 409 time of the of the manifold tracing algorithm. The reconstructed manifold in the tests is the n -
 410 dimensional sphere embedded in \mathbb{R}^d . The ambient triangulation used is a Coxeter triangulation of
 411 type \tilde{A}_d . The diameter of the full simplices is fixed for all d .

406 Coxeter triangulation is beneficial in practice as it produces a smaller output in less time
 407 (see Proposition 10).

423 In Figure 4, we present a PL approximation of a two-dimensional flat torus without
 424 boundary embedded in \mathbb{R}^{10} built by the manifold tracing algorithm. The torus has been
 425 rotated and translated in \mathbb{R}^{10} so that the coordinate axes do not play any special role. Note
 426 that there is no C^2 isometric embedding of the flat torus in \mathbb{R}^3 .



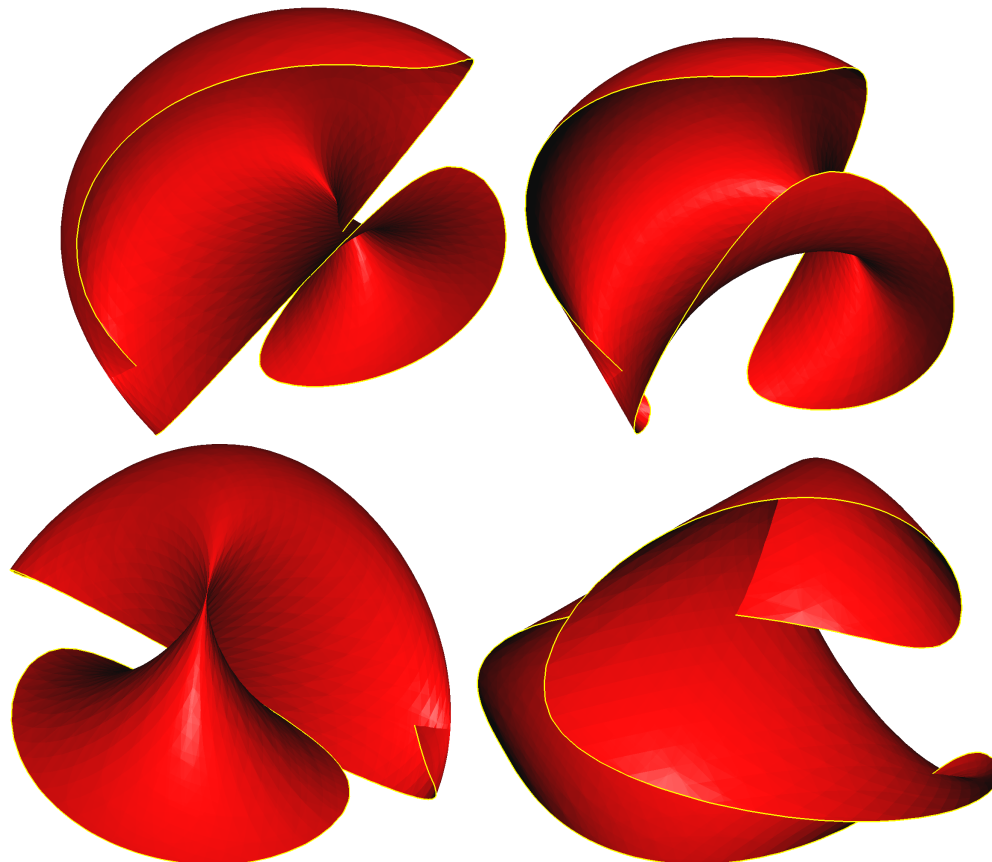
412 **Figure 3** Comparison of the size of the output of the manifold tracing algorithm using two
 413 types of ambient triangulations: a Coxeter triangulation of type \tilde{A}_d (in blue), and the Freudenthal-
 414 Kuhn triangulation of \mathbb{R}^d (in red) with the same diameter $0.07\sqrt{d}$ of d -dimensional simplices. The
 415 reconstructed manifold is the 2-dimensional implicit surface “Chair” embedded in \mathbb{R}^d given by the
 416 equations: $(x_1^2 + x_2^2 + x_3^2 - 0.8)^2 - 0.4((x_3 - 1)^2 - 2x_1^2)((x_3 + 1)^2 - 2x_2^2) = 0$, and $x_i = 0$ for $i > 3$.



417 **Figure 4** The piecewise-linear approximation of a flat torus embedded in \mathbb{R}^{10} defined by the
 418 equations $x_1^2 + x_2^2 = 1$, and $x_3^2 + x_4^2 = 1$, and $x_i = 0$ for $i > 4$, projected to \mathbb{R}^3 . The ambient
 419 triangulation used is a Coxeter triangulation of type \tilde{A}_{10} with the diameter of the full-dimensional
 420 simplices 0.23. The output size $|S|$ is 509 952. The execution time of the algorithm is 231s. The
 421 torus has been rotated and translated in \mathbb{R}^{10} so that the coordinate axes do not play any special
 422 role.

427 **4.2 Manifolds with boundary**

428 The algorithm has been adapted to handle submanifolds with boundary and surfaces with a
 429 piecewise smooth boundary, see Appendix 3.5. In Figure 5, we present the mesh obtained by
 430 our algorithm on a portion of a flat torus embedded in \mathbb{R}^4 , and cut by a hypersphere. The
 431 torus has been rotated and translated in \mathbb{R}^4 so that the coordinate axes do not play any
 432 special role.



433 ■ **Figure 5** Four views of the flat torus in \mathbb{R}^4 given by two equations $x_1^2 + x_2^2 = 1$, and $x_3^2 + x_4^2 = 1$ cut
 434 by the hypersphere $(x_1 - 1)^2 + x_2^2 + (x_3 - 1)^2 + x_4^2 = 4$, projected to \mathbb{R}^3 . The ambient triangulation used
 435 is a Coxeter triangulation of type A_4 with the diameter 0.15 of the full-dimensional simplices. The
 436 reconstructed boundary is highlighted in yellow. The size $|\mathcal{S}|$ of the piecewise-linear approximation
 437 is 14 779. The execution time of the algorithm is 1.84s. The torus has been rotated and translated
 438 in \mathbb{R}^4 so that the coordinate axes do not play any special role.

439 **4.3 An application in algebraic geometry**

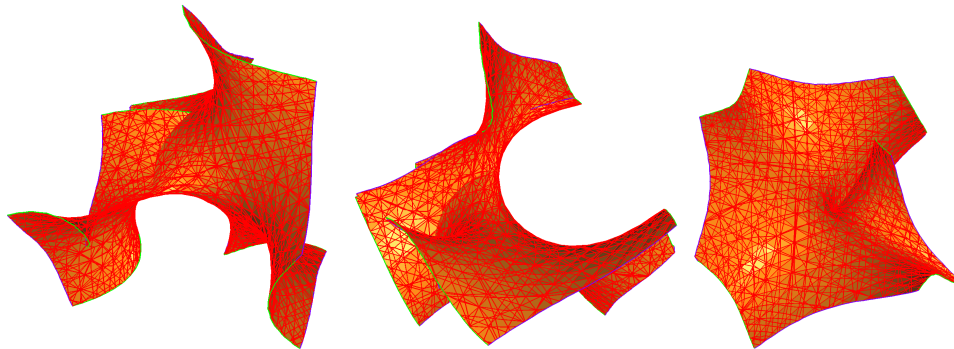
440 We also applied our algorithm to a more complicated example of interest in algebraic
 441 geometry [4] where an active field of research is to understand the geometry and topology
 442 of various projective varieties. Projective varieties are isomanifolds defined by polynomial
 443 equations in the complex projective space $\mathbb{C}\mathbb{P}^d = (\mathbb{C}^{d+1} \setminus 0) / \mathbb{C}^*$ of complex dimension d .
 444 One such example is the complex one-dimensional curve (that is a real dimensional surface)
 445 given by the equation $z_1^2 \bar{z}_2 + z_2^2 \bar{z}_3 + z_3^2 \bar{z}_1 = 0$ in $\mathbb{C}\mathbb{P}^2$, where \bar{z} denotes the conjugate of the
 446 complex number z .

447 To be able to apply our algorithm, we first need to pass from homogenous coordinates
 448 $[z_1 : \dots : z_{d+1}]$ on \mathbb{CP}^d to affine coordinates $[z'_1 : \dots : z'_{i-1} : 1 : z'_{i+1} : \dots : z'_{d+1}]$ by picking
 449 the i th coordinate to be equal to 1, that is $z'_j = z_j/z_i$. Given some homogenous coordinates
 450 $[z_1 : \dots : z_{d+1}]$, we can choose the i th coordinate to be set to 1 to be the coordinate whose
 451 absolute value is the largest, so that \mathbb{CP}^d can be written as the union of the $d + 1$ sets
 452 $\{[z'_1 : \dots : z'_{i-1} : 1 : z'_{i+1} : \dots : z'_{d+1}] \mid |z'_j| \leq 1\}$, with the boundaries of these sets identified.
 453 Writing $z'_j = x_j + iy_j$ these sets are (seen as real sets) identical to the domain of \mathbb{R}^{2d}

454
$$D_i = \{(x_1, y_1, \dots, x_{i-1}, y_{i-1}, x_{i+1}, y_{i+1}, \dots, x_{d+1}, y_{d+1}) \mid x_j^2 + y_j^2 \leq 1\}.$$

455 Let f be a homogenous polynomial in $d + 1$ complex variables and their complex conjugates.
 456 For each i , we can fix the i th coordinate to be 1. Writing each variable in terms of its real
 457 and imaginary part yields a real inhomogeneous polynomial in $2d$ (real) variables on the
 458 domain D_i . Taking the real and imaginary parts of the function yields two real functions
 459 $f_{\Re,i}$ and $f_{\Im,i}$ on D_i . As real sets, the projective variety $f = 0$ on \mathbb{PC}^d and the intersection
 460 of the sets $f_{\Re,i} = 0$ and $f_{\Im,i} = 0$ on D_i for each i (with the boundaries identified) are the
 461 same. We can therefore apply the tracing algorithm to each isomanifold ($f_{\Re,i} = 0, f_{\Im,i} = 0$)
 462 of D_i independently. Since their boundaries coincide, we can then glue these isomanifolds
 463 along their boundary to obtain a PL-approximation of the projective variety $f = 0$. This, for
 464 example, allows to recover the Euler characteristic of $f = 0$ on \mathbb{PC}^d .

465 This principle generalizes to varieties of higher codimension, that is to varieties defined
 466 by a number of homogenous polynomials f_1, \dots, f_{d-m} .



467 **Figure 6** The three triangulated surfaces as discussed in the example of $z_1^2 \bar{z}_2 + z_2^2 \bar{z}_3 + z_3^2 \bar{z}_1 = 0$
 468 in \mathbb{PC}^2 after projection from \mathbb{R}^4 to \mathbb{R}^3 .

469 We illustrate the above construction on the above equation $z_1^2 \bar{z}_2 + z_2^2 \bar{z}_3 + z_3^2 \bar{z}_1 = 0$ in
 470 \mathbb{PC}^2 . By passing to affine coordinates, we recover $z_1^2 \bar{z}_2 + z_2^2 + \bar{z}_1 = 0$, $z_1^2 + \bar{z}_3 + z_3^2 \bar{z}_1 = 0$, and
 471 $\bar{z}_2 + z_2^2 \bar{z}_3 + z_3^2 = 0$. By expanding $z_1 = x_1 + iy_1$, $z_2 = x_2 + iy_2$, and $z_3 = x_3 + iy_3$, we find two real
 472 equations for each of the complex equations. We give those corresponding to $z_1^2 \bar{z}_2 + z_2^2 + \bar{z}_1 = 0$,
 473 the other equations being symmetric. For this complex equation, we get the real equations
 474 $x_1 + x_1^2 x_2 + x_2^2 - x_2 y_1^2 + 2x_1 y_1 y_2 - y_2^2 = 0$ and $-y_1 + 2x_1 x_2 y_1 - x_1^2 y_2 + 2x_2 y_2 + y_1^2 y_2 = 0$ in
 475 \mathbb{R}^4 . The domain D_3 is in this case determined by the equations $x_1^2 + y_1^2 \leq 1$ and $x_2^2 + y_2^2 \leq 1$.
 476 Hence we find a surface in \mathbb{R}^4 with a piecewise smooth boundary. The result provided by
 477 our algorithm is shown in Figure 6. For visualization purposes, we show the three surfaces
 478 separately and projected from \mathbb{R}^4 to \mathbb{R}^3 .

479 **5 Conclusion and open questions**

480 We have presented an efficient, practical and provably correct algorithm to compute the
 481 PL-approximation of an isomanifold of any dimension and codimension. Since isomanifolds
 482 are a special type of manifolds, it is tempting to see if our algorithm extends to general
 483 smooth submanifolds of \mathbb{R}^d .

484 The manifold tracing algorithm itself is quite general and works for any submanifold as
 485 soon as we provide a seed point and an oracle that can determine whether a k -simplex of
 486 the ambient triangulation intersects \mathcal{M} or not. In this general setting, the simple algorithm
 487 described above is sufficient to compute a PL-approximation of the manifold and satisfies
 488 the bounds given in Section 3.

489 However, this is not enough to obtain guarantees on the geometric and topological quality
 490 of the output mesh. Such guarantees can be obtained by slightly perturbing the ambient
 491 Coxeter triangulation of type \tilde{A}_d so that the following conditions are satisfied:

- 492 1. All k -dimensional faces τ in \mathcal{T} , with $k \leq d - n - 1$, are far enough from \mathcal{M} .
- 493 2. The longest edge length of \mathcal{T} is upper bounded and its smallest thickness is lower bounded.

494 Under these conditions, Algorithm 1 will output a PL-approximation that is topologically
 495 equivalent and close in Hausdorff distance to the input manifold [7]. However, in the worst
 496 case, we need to perturb all the simplices of \mathcal{T} of dimension less than the codimension
 497 $d - n$ that are incident on a vertex. Since there are exponentially many such simplices, such
 498 methods have a complexity that depends exponentially on the ambient dimension d , and
 499 have not proved useful in practice except in some simple cases. It remains open whether
 500 general smooth manifolds embedded in \mathbb{R}^d can be triangulated in time polynomial in d as we
 501 were able to do here in the special case of isomanifolds.

502 — **References** —

- 503 1 Eugene Allgower and Kurt Georg. Estimates for piecewise linear approximations of implicitly
504 defined manifolds. *Applied Mathematics Letters*, 2(2):111–115, 1989.
- 505 2 Eugene Allgower and Kurt Georg. *Numerical continuation methods: an introduction*, volume 13.
506 Springer Science & Business Media, 1990.
- 507 3 Eugene Allgower and Phillip H. Schmidt. An algorithm for piecewise-linear approximation of
508 an implicitly defined manifold. *SIAM journal on numerical analysis*, 22(2):322–346, 1985.
- 509 4 Aurélien Alvarez and Bertrand Deroin. Dynamique et topologie du feuilletage de Jouanolou.
510 Preprint, 2019.
- 511 5 Jean-Daniel Boissonnat, Frédéric Chazal, and Mariette Yvinec. *Geometric and Topological*
512 *Inference*. Cambridge Texts in Applied Mathematics. Cambridge University Press, 2018.
513 doi:10.1017/9781108297806.
- 514 6 Jean-Daniel Boissonnat and Arijit Ghosh. Manifold reconstruction using tangential Delaunay
515 complexes. *Discrete & Computational Geometry*, 51(1):221–267, 2014.
- 516 7 Jean-Daniel Boissonnat, Siargey Kachanovich, and Mathijs Wintraecken. Triangulating
517 submanifolds: An elementary and quantified version of Whitney’s method. hal-01950149,
518 December 2018.
- 519 8 Jean-Daniel Boissonnat, Siargey Kachanovich, and Mathijs Wintraecken. A compact data
520 structure for high dimensional Coxeter-Freudenthal-Kuhn triangulations. Submitted to the
521 International Symposium on Computational Geometry (SoCG2021), 2020.
- 522 9 Jean-Daniel Boissonnat, Siargey Kachanovich, and Mathijs Wintraecken. Tracing isomanifolds
523 in \mathbb{R}^d in time polynomial in d . Submitted to the International Symposium on Computational
524 Geometry (SoCG2021), 2020.
- 525 10 Jean-Daniel Boissonnat and Mathijs Wintraecken. The topological correctness of PL-
526 approximations of isomanifolds. In *34th International Symposium on Computational Ge-*
527 *ometry, SoCG 2020, June 23-26, 2020, Zurich, Switzerland.*, 2020. Full version. URL:
528 <https://hal.inria.fr/hal-02386193>.
- 529 11 Yen-Chi Chen. Solution manifold and its statistical applications, 2020. arXiv:2002.05297.
530 arXiv:2002.05297.
- 531 12 Siu-Wing Cheng, Tamal K Dey, and Edgar A Ramos. Manifold reconstruction from point
532 samples. In *SODA*, volume 5, pages 1018–1027, 2005.
- 533 13 Aruni Choudhary, Siargey Kachanovich, and Mathijs Wintraecken. Coxeter triangulations
534 have good quality. *Mathematics in Computer Science*, 14:141–176, 2020. URL: <https://doi.org/10.1007/s11786-020-00461-5>.
- 535 14 Kenneth L. Clarkson. Tighter bounds for random projections of manifolds. In *Proceedings*
536 *of the 24th ACM Symposium on Computational Geometry, College Park, MD, USA, June*
537 *9-11, 2008*, pages 39–48, 2008. URL: <https://doi.org/10.1145/1377676.1377685>, doi:
538 10.1145/1377676.1377685.
- 539 15 David P. Dobkin, Allan R. Wilks, Silvio V. F. Levy, and William P. Thurston. Contour tracing
540 by piecewise linear approximations. *ACM Transactions on Graphics (TOG)*, 9(4):389–423,
541 1990.
- 542 16 J. J. Duistermaat and J. A. C. Kolk. *Multidimensional Real Analysis I: Differentiation*.
543 Number 86 in Cambridge Studies in Advanced Mathematics. Cambridge University Press,
544 2004.
- 545 17 B. Curtis Eaves. *A course in triangulations for solving equations with deformations*, volume
546 234. Lecture Notes in Economics and Mathematical Systems, 1984.
- 547 18 Armin Eftekhari and Michael B. Wakin. What happens to a manifold under a bi-lipschitz
548 map? *Discrete & Computational Geometry*, 57(3):641–673, 2017. URL: [https://doi.org/10.](https://doi.org/10.1007/s00454-016-9847-6)
549 [1007/s00454-016-9847-6](https://doi.org/10.1007/s00454-016-9847-6), doi:10.1007/s00454-016-9847-6.
- 550 19 A. Gomes, I. Voiculescu, J. Jorge, B. Wyvill, and C. Galbraith. *Implicit Curves and Surfaces:*
551 *Mathematics, Data Structures and Algorithms*. Springer, 2009.
- 552

- 553 20 GUDHI Project "<http://gudhi.gforge.inria.fr/doc/latest/>" . URL: <http://gudhi.gforge.inria.fr/doc/latest/>.
- 554
- 555 21 Siargey Kachanovich. *Meshing submanifolds using Coxeter triangulations*. Theses, COMUE Université Côte d'Azur (2015 - 2019), October 2019. URL: <https://hal.inria.fr/tel-02419148>.
- 556
- 557 22 William E. Lorensen and Harvey E. Cline. Marching cubes: A high resolution 3d surface construction algorithm. *ACM siggraph computer graphics*, 21(4):163–169, 1987.
- 558
- 559 23 Chohong Min. Simplicial isosurfacing in arbitrary dimension and codimension. *Journal of Computational Physics*, 190(1):295–310, 2003.
- 560
- 561 24 Timothy S. Newman and Hong Yi. A survey of the marching cubes algorithm. *Computers & Graphics*, 30(5):854 – 879, 2006. URL: <http://www.sciencedirect.com/science/article/pii/S0097849306001336>, doi:<https://doi.org/10.1016/j.cag.2006.07.021>.
- 562
- 563
- 564 25 James M Ortega and Werner C Rheinboldt. *Iterative solution of nonlinear equations in several variables*. SIAM, 2000.
- 565
- 566 26 Alexander M Ostrowski. *Solution of Equations and Systems of Equations: Pure and Applied Mathematics: A Series of Monographs and Textbooks, Vol. 9*, volume 9. Elsevier, 2016.
- 567
- 568 27 Michael J. Todd. *The computation of fixed points and applications*, volume 124. Lecture Notes in Economics and Mathematical Systems, 1976.
- 569
- 570 28 Nakul Verma. A note on random projections for preserving paths on a manifold. Technical Report Tech. Report CS2011-0971, UC San Diego, 2011.
- 571
- 572 29 Rephael Wenger. *Isosurfaces: geometry, topology, and algorithms*. AK Peters/CRC Press, 2013.
- 573
- 574 30 H. Whitney. *Geometric Integration Theory*. Princeton University Press, 1957.

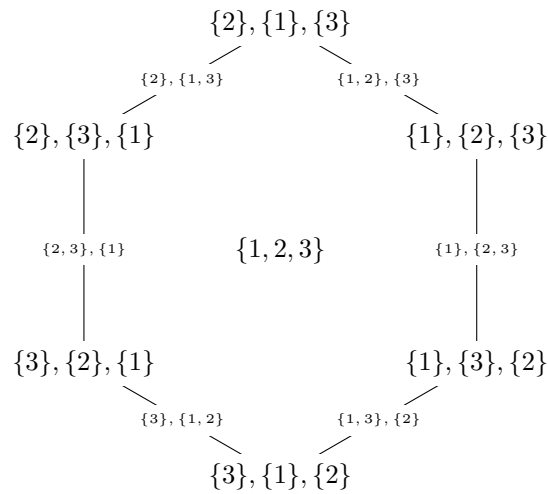
575 **A Permutahedra**

576 We write $[i] = \{1, \dots, i\}$, and $[i, j] = \{i, \dots, j\}$.

577 **Definition 14** (Permutahedron). *A d -permutahedron is a d -dimensional polytope, which is*
 578 *the convex hull \mathcal{P} of all points in \mathbb{R}^{d+1} , the coordinates of which are permutations of $[d + 1]$.*
 579 *Formally, this convex hull can be written as:*

580
$$\mathcal{P} = \text{conv}\{(\sigma(1), \dots, \sigma(d + 1)) \in \mathbb{R}^{d+1} \mid \sigma \in \mathfrak{S}_{d+1}\},$$

581 where \mathfrak{S}_{d+1} denotes the set of permutations of $[d + 1]$.



582 **Figure 7** The 2-permutahedron and the ordered partitions associated to its faces.

583 The following two corollaries are proved in [9].

584 **Corollary 15.** *The number of facets of an i -face σ of a d -permutahedron is at most 2^{i+1} .*

585 **Corollary 16.** *Let $p_{i,j}$ denote the number of i -faces of a j -face of the d -permutahedron.*
 586 *We have $p_{i,j} \leq \frac{1}{2^{\min(i,d-i)}} \binom{j}{i} (j + 1)!$*

587 **B Proofs**

588 **Proof of Proposition 9.** The complexity of the initialization is $O(d)$. The complexity of each
 589 iteration of the while loop consists of computing the cofacets of the popped k -dimensional
 590 simplex in the queue, computing facets of these cofacets, and applying the intersection oracle
 591 on each of these facets. An upper bound on the number of cofacets of a k -simplex in a
 592 CFK-triangulation follows, by duality, from Corollary 15, specifically $O(2^n)$. Each of these
 593 cofacets has $k + 2$ facets. Therefore, for each iteration of the while loop, the algorithm applies
 594 the intersection oracle on $O(k2^n)$ simplices. By using this observation, and the complexities
 595 in Lemmas 3, and 4, the total time complexity of each iteration of the while loop follows:

596
$$O(d2^n) + O(dk2^n) + O(k2^n I) = O(k2^n(d + I)) = O(k2^n I).$$

597 Since there are $|\mathcal{S}|$ iterations of the while loop, the result follows. ◀

598 **Proof of Proposition 10.** By the definition of CFK-triangulations in Section 2.1, \mathcal{T} is an
 599 arrangement of $d(d-1)/2$ families H_u of hyperplanes, $u \in E_{\mathcal{T}}$. Each family H_u consists of
 600 the hyperplanes $H_{u,k}$, $k \in \mathbb{Z}$, all orthogonal to u . Let $L_{\mathcal{T}}$ be the length of the longest edge
 601 of a simplex in \mathcal{T} and $R_{\mathcal{T}}$ be the maximal norm of the vectors u . Note that the distance
 602 between two consecutive hyperplanes in family H_u is $1/\|u\| \geq 1/R_{\mathcal{T}}$.

603 We will rescale the arrangement of hyperplanes so that the maximal diameter of the
 604 simplices is D , the required precision. Hence the distance between two consecutive hyperplanes
 605 in H_u is $D/(L_{\mathcal{T}}\|u\|)$. It follows that at most $\sqrt{d}L_{\mathcal{T}}\|u\|/D$ hyperplanes of family H_u intersect
 606 the unit cube C_d that contains \mathcal{M} (which has diameter \sqrt{d}). Consider any subset of n
 607 families among the $d(d-1)/2$ families, and write I for the associated subset of indices,
 608 $I \subset [1, d(d-1)/2]$, $|I| = n$. Now take n hyperplanes, one in each family H_{u_i} , $i \in I$. Their
 609 common intersection is an affine space of dimension $k = d - n$. This affine space intersects \mathcal{M}
 610 in at most K points under the general position assumption and the fact that \mathcal{M} is K -sparse.
 611 The total number of intersection points $N_{\mathcal{T}} = \mathcal{T}_k \cap \mathcal{M}$ is thus bounded as follows

$$612 \quad N_{\mathcal{T}} \leq K \binom{d(d-1)/2}{n} \times \prod_{i \in I} \frac{\sqrt{d}L_{\mathcal{T}}\|u_i\|}{D} \leq \frac{K}{n!} \times \left(\frac{d^2\sqrt{d}L_{\mathcal{T}}R_{\mathcal{T}}}{2D} \right)^n. \quad (2)$$

613 Here the binomial coefficient arises as the number of choices of n families of hyperplanes.
 614 Consider now more specifically Coxeter triangulations of type \tilde{A}_d and FK -triangulations.
 615 It follows from Section 2.1 that $R_C = R_{FK} = \sqrt{2}$. The longest edge L_{FK} in a Freudenthal-
 616 Kuhn triangulation has length at most (in fact exactly) \sqrt{d} since each simplex is contained
 617 in a cubical cell of the d -dimensional unit grid. Furthermore, it is proved in [13, point 6 of
 618 \tilde{A}_d in Section 6] that the longest edge length in the Coxeter triangulation of type \tilde{A}_d is

$$619 \quad L_C = \begin{cases} \frac{\sqrt{d+1}}{2} & \text{if } d \text{ is odd,} \\ \frac{1}{2} \sqrt{\frac{d(d+2)}{(d+1)}} & \text{if } d \text{ is even,} \end{cases} \quad (3)$$

620 and hence $L_C < \frac{\sqrt{d+2}}{2}$. We then deduce from (2)

$$621 \quad N_C \leq \frac{K}{n!} \times \left(\frac{d^2\sqrt{d(d+2)}}{2\sqrt{2}D} \right)^n$$

$$622 \quad N_{FK} \leq \frac{K}{n!} \times \left(\frac{d^3}{\sqrt{2}D} \right)^n.$$

623 ◀

624 **Proof of Proposition 11.** Let σ be a k -simplex of a CFK-triangulation that intersects $\hat{\mathcal{M}}$,
 625 and let σ^* be its dual cell. By definition, σ^* is a m -dimensional face of \mathcal{T}^* , the polytopal cell
 626 complex dual to \mathcal{T} . The collection of all σ^* associated to the k -simplices σ of \mathcal{T} that intersect
 627 $\hat{\mathcal{M}}$ form a cell complex $\hat{\mathcal{M}}^*$ dual to $\hat{\mathcal{M}}$. To bound the number of faces of all dimensions of
 628 the PL-approximation $\hat{\mathcal{M}}$, it is therefore sufficient to bound the number of faces of $\hat{\mathcal{M}}^*$.

629 Each d -dimensional cell in \mathcal{T}^* is a permutahedron (Proposition 2). Hence, σ^* is a n -face
 630 of a d -permutahedron. The number of faces of σ^* of dimensions 0 to $n-1$ (or equivalently
 631 the number of cofaces of σ of dimensions $n+1$ to d) is:

$$632 \quad \sum_{i=0}^{n-1} p_{i,n} \leq \sum_{i=0}^{n-1} \frac{1}{2^i} \binom{n}{i} (n+1)! = \frac{3^n - 1}{2^n} (n+1)!$$

633 where $p_{i,j}$ denotes the number of i -faces of a j -face of the d -permutahedron and is bounded
634 in Corollary 16. The last equality can be easily verified using Mathematica. The overall
635 combinatorial complexity of $\hat{\mathcal{M}}$ is therefore

$$636 \quad |\mathcal{S}| \times \frac{3^n - 1}{2^n} (n + 1)!,$$

637 where \mathcal{S} is bounded in Proposition 10. ◀